Magnetic assembly of Eu-doped $NaYF_4$ nanorods for field-responsive linearly and circularly polarized luminescence

Zhongxiang Wang, David Schnable, Qingsong Fan, Zhiwei Li, Gaël Ung, Yadong Yin**

Corresponding Authors

Yadong Yin − Department of Chemistry, University of California, Riverside, California 92521, United States; orcid.org/0000-0003-0218-3042; Email: yadong.yin@ucr.edu

Gaël Ung − Department of Chemistry, University of Connecticut, Storrs, Connecticut 06269, United States; orcid.org/0000-0002-6313-3658; Email: gael.ung@uconn.edu

Authors

Zhongxiang Wang − Department of Chemistry, University of California, Riverside, California 92521, United States; orcid.org/0009-0004-4870-0767

David Schnable − Department of Chemistry, University of Connecticut, Storrs, Connecticut 06269, United States; orcid.org/0000-0002-8650-997X

Qingsong Fan − Department of Chemistry, University of California, Riverside, California 92521, United States; orcid.org/0000-0001-8555-769X

Zhiwei Li − Department of Chemistry, University of California, Riverside, California 92521, United States; orcid.org/0000-0002-1489-4506

ABSTRACT: Colloidal assembly has emerged as an effective avenue for achieving polarized light emission. Here, we showcase the efficacy and versatility of magnetic colloidal assembly in enabling both linearly and circularly polarized luminescence. Colloidal europium-doped $NaYF_4$ nanorods with surface-bound Fe_3O_4 nanoparticles are magnetically assembled into linear or chiral superstructures using corresponding fields created in permanent magnets. In a uniform magnetic field generated by opposing poles, the assemblies exhibit photoluminescence with intensity tunable in response to the magnetic field direction, higher when the nanorods are perpendicular to light propagation than when they are parallel. The obtained superstructures display strong linearly polarized luminescence when the nanorods are aligned vertically, exhibiting a high degree of polarization up to 0.61. In a quadrupole chiral field generated by permanent magnets, the assemblies emit left-handed or right-handed polarized light depending on the position of sample placement, attaining a g-factor of 0.04. Furthermore, the superstructures immobilized in a hydrogel film are found to retain their chirality, exhibiting opposite chiroptical responses depending on the sample orientation. The magnetic colloidal assembly approach facilitates the convenient and efficient generation of polarized light emissions from non-magnetic luminescent materials, thus creating opportunities for tailoring light behavior in developing innovative optoelectronic devices.

KEYWORDS: self-assembly, magnetic field, chirality, circularly polarized luminescence, linearly polarized luminescence

INTRODUCTION

Light polarization has important applications for display,[1] imaging,[2] sensing,[3] actuation,[4] and information storage.[5-6] The polarization state of light can assume various forms—linear, circular, or elliptical, contingent upon the direction in which the electric field oscillates. Theoretically, the light emitted by any phosphor contains a certain amount of polarized light, including linearly and circularly polarized light. By assembling the phosphors into a well-aligned orientation or specific configurations, the polarization of emitted light could be greatly magnified.[7-8] Various self-assembly methods have been reported to transform the unpolarized emission into linear or circular polarization using anisotropic alignment or chirality transfer between chiral templates and luminescent phosphors.[9-10] For example, lanthanide-doped $NaYF_4$ upconversion nanorods were aligned on silicon substrates by a shear force-driven method, producing superstructures showing linearly polarized luminescence (LPL) with a high degree of polarization.[11] In addition, perovskite and lanthanide-doped upconversion nanoparticles (NPs) were co-assembled with chiral organic nanotube templates to exhibit circularly polarized luminescence (CPL).[12-13]

As a non-template approach, magnetic assembly has been widely employed for organizing nanoscale building blocks into diverse superstructures with controllable symmetries and phases.[14-16] It features many advantages, including instantaneous and reversible action, contactless operation, and the directional nature of magnetic interactions.[1, 17-20] Recent studies have further revealed that the magnetic field can be configured as uniform or chiral depending on the spatial arrangement of magnets, enabling the creation of chiral superstructures through the magnetic assembly approach.[21-23] Applying this approach to luminescent nanostructures is therefore expected to produce superstructures featuring polarized emission, with dynamic tunability offered by the convenient manipulation of the strength and direction of the magnetic field.

In this study, we demonstrate the successful magnetic assembly of inorganic fluorescent nanorods into superstructures capable of producing linearly and circularly polarized luminescence. Lanthanide-doped $NaYF_4$ was chosen as the fluorescent component due to its high stability, narrow emission band, long emission lifetime, and the capacity for polarization-dependent luminescence enabled by the anisotropic crystalline environment surrounding the emitter.[24] It was synthesized in the form of colloidal nanorods, which were then made magnetically responsive by coating their surface with a thin layer of Fe_3O_4 nanoparticles. We show that the fluorescence intensity and polarization properties of the assemblies can be controlled by the direction and chirality of the applied magnetic field, leading to tunable linearly or circularly polarized luminescence. Notably, the degree of polarization reached up to 0.61 for LPL, while the luminescence dissymmetry factor, g_{lum}, attained values up to 0.04 for CPL. Moreover, we demonstrate that the chiral superstructures can be fixed in hydrogel films to exhibit an unusual chiroptical inversion property upon flipping the samples.

RESULTS AND DISCUSSION

The Europium (Eu)-doped $NaYF_4$ (Eu-$NaYF_4$) nanorods (NRs) were prepared by a hydrothermal method using oleic acid as a capping ligand,[11] featuring a hydrophobic surface and an average length of 530 nm and aspect ratio of 10 (**Figure 1a**). Under optimal excitation at 394 nm, the Eu-$NaYF_4$ nanorods showed strong photoluminescence (PL) at 591 nm, 614 nm, and 694 nm, corresponding to the energy transition of $^5D_0 \rightarrow {}^7F_1$, $^5D_0 \rightarrow {}^7F_2$, and $^5D_0 \rightarrow {}^7F_4$ in Eu^{3+}, respectively (**Figure S1**). The hydrophobic Eu-$NaYF_4$ NRs were transferred to the aqueous phase by being treated with a commonly used phase transfer agent, tetramethyl ammonium hydroxide (TMAH), which could replace the original oleic acid ligands.[25-26] Magnetic Fe_3O_4 NPs with an average size of around 8.7 nm (**Figure S2**), prepared through co-precipitating the Fe(III) and Fe(II) in the

presence of OH^-,[27] were incorporated onto the surface of Eu-$NaYF_4$ NRs to enable the magnetic response of the composite nanorods to external fields.[28-33] Poly (methacrylic acid) (PMAA) containing carboxylic groups was used as a coupling agent, first coating the $NaYF_4$ NRs with a thickness of around 10 nm (**Figure 1b**) and then binding to Fe_3O_4 NPs through a strong coordination between COO^- and Fe(II)/Fe(III).[34] After removing free Fe_3O_4 NPs by repeated centrifugation at a proper speed (see details in Supporting Information), a thin layer of Fe_3O_4 NPs was retained on the nanorod surface, as shown in **Figure 1c**. Low-magnification TEM images of Eu-$NaYF_4$@PMAA and Eu-$NaYF_4$@PMAA@ Fe_3O_4 structures were shown in **Figure S3** and **Figure 1d**, respectively, indicating no serious agglomeration throughout the surface treatment process.

The absorption spectra and PL intensity were monitored throughout the surface treatment and coating process at an Eu-$NaYF_4$ concentration of 1 mg/mL, as shown in **Figure S4a** and **Figure 1e**, respectively. After phase transfer, the PL intensity increased, likely due to both the removal of oleic acid layers on the $NaYF_4$ nanorod surface, which could inhibit the emission,[35-36] and the stronger optical absorption (**Figure S4a**). This is consistent with a recent report on the influence of oleic acid removal on the optical properties of lanthanide-doped nanocrystals.[37] After PMAA coating, the PL intensity slightly decreased due to the absorption of light by the polymer layer. After Fe_3O_4 coating in a thin layer, the PL intensity significantly decreased because of the intensive absorption of visible light by Fe_3O_4 NPs (**Figure S4b**). The presence of a dense coating of Fe_3O_4 nanoparticles led to a more pronounced reduction in PL intensity, as illustrated in **Figure S5**. Thanks to the initial strong PL of Eu-$NaYF_4$, the composite nanorods could emit PL with sufficient intensity for further investigations. Magnetic hysteresis measurements were conducted on the Fe_3O_4 nanoparticles and the Eu-$NaYF_4$@PMAA@Fe_3O_4 composite nanorods (**Figure 1f)**. Both

samples exhibited S-shaped curves with minimal hysteresis loops, indicating their superparamagnetic nature and confirming their suitability for colloidal assembly under the magnetic field. However, upon exposure to a magnetic field for an extended period, the composite nanorods in the aqueous dispersion would eventually aggregate, leading to significant PL quenching (**Figure S6**).

To bolster the colloidal stability of the assemblies within magnetic fields, we employed polyols as solvents due to their higher viscosities compared to water (**Table S1**). Indeed, the magnetic separation of the composite nanorods from the dispersion took the longest time in tetraethylene glycol (TEG) due to its highest viscosity among all polyols. **Figure 1g** evaluates the PL intensities of Eu-$NaYF_4$@PMAA@Fe_3O_4 nanorods with the concentration of 1 mg/mL of Eu-$NaYF_4$ in these polyols. Compared with water, the polyol solvents could quench the PL to a certain degree due to abundant OH groups.[38] From EG to diethylene glycol (DEG), triethylene glycol (TriEG), and TEG, PL increased largely because of the reduced chelating effect of the two OH groups as the carbon chain prolonged.[39] Thus, TEG was selected as the solvent in this study due to its minimum PL quenching and highest viscosity.

We compared PL at various concentrations of composite nanorods in TEG to ascertain the optimal concentrations, as shown in **Figure 1h**. The highest PL intensity was obtained at a concentration of around 2 mg/mL Eu-$NaYF_4$, which resulted from the interplay between Eu-$NaYF_4$ emission and Fe_3O_4 absorption. While the PL was weak when the phosphor concentration was below 2 mg/mL, a higher nanorod concentration would result in stronger magnetic interactions, consequently accelerating particle agglomeration and leading to PL quenching. Therefore, TEG dispersions of the composite nanorods at 2 mg/mL Eu-$NaYF_4$ concentration were chosen for further studies.

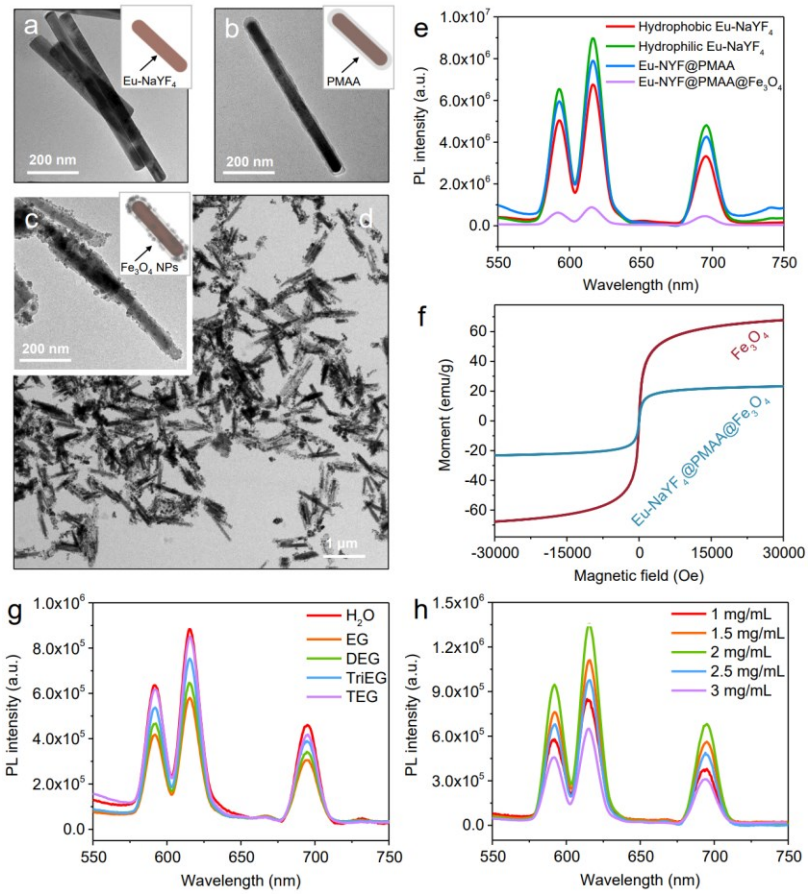

Figure 1. (a-d) TEM images of Eu-$NaYF_4$ nanorods: (a) after transferring into aqueous phase by TMAH treatment; (b) after PMAA coating; (c-d) after surface decoration with Fe_3O_4 nanoparticles at different magnifications; (e) PL spectra of Eu-$NaYF_4$ nanorods throughout the surface treatment process in a concentration of 1 mg/mL; (f) The magnetic hysteresis curve of Fe_3O_4 nanoparticles and Eu-$NaYF_4$@PMAA@Fe_3O_4 composite nanorods; (g) PL spectra of composite nanorods dispersed in different solvents, with an Eu-$NaYF_4$ concentration of 1 mg/mL; (h) PL spectra of composite nanorods dispersed in TEG in different concentrations. The insets in (a-c) are schematic illustrations of the corresponding nanostructures.

It is recently discovered that a cubic permanent magnet can generate a quadrupole chiral magnetic field due to constant field rotation.[23] **Figure 2a** shows the simulated magnetic field distribution of

a cubic magnet, with region I corresponding to a uniform magnetic field and regions II and III exhibiting left-handed and right-handed chirality, respectively. We have recently shown that the chirality of the magnetic field can be transferred to non-magnetic species by attaching them to magnetic nanoparticles and then assembling the nanocomposites within the field.[40] As a result, the assembly of composite nanorods in uniform or chiral magnetic fields is expected to produce linear or left/right-handed chiral superstructures, depending on their spatial location within the field. We assessed the alignment of the composite nanorods under both a chiral (**Figure 2b**) and a uniform magnetic field (**Figure 2c**). While most nanorods follow the field direction, there are a small number of unaligned nanorods in both samples, as indicated by the solid arrows. The extent of alignment was estimated to be 0.94 and 0.96 under a chiral and uniform magnetic field, respectively, by quantifying the nanorods aligned parallel to the magnetic field direction and dividing this count by the total number of nanorods within the marked squares.

The alignment of Eu-$NaYF_4$@PMAA@Fe_3O_4 composite nanorods in solution could be precisely controlled by tuning the direction of the external magnetic field (**Figure S7**). We observed simultaneous changes in PL intensity in response to an external magnetic field. As shown in **Figure 2d**, in the 90^o setup of PL measurement (with the detector at 90^o to the excitation source), the PL intensity of the assemblies varied with the magnetic field direction. When the nanorods were aligned parallel to the detector direction (x-axis) or vertical direction (z-axis), the PL intensity of the assemblies was stronger than that when they were along the excitation direction (y-axis) or in random orientation without the magnetic field.

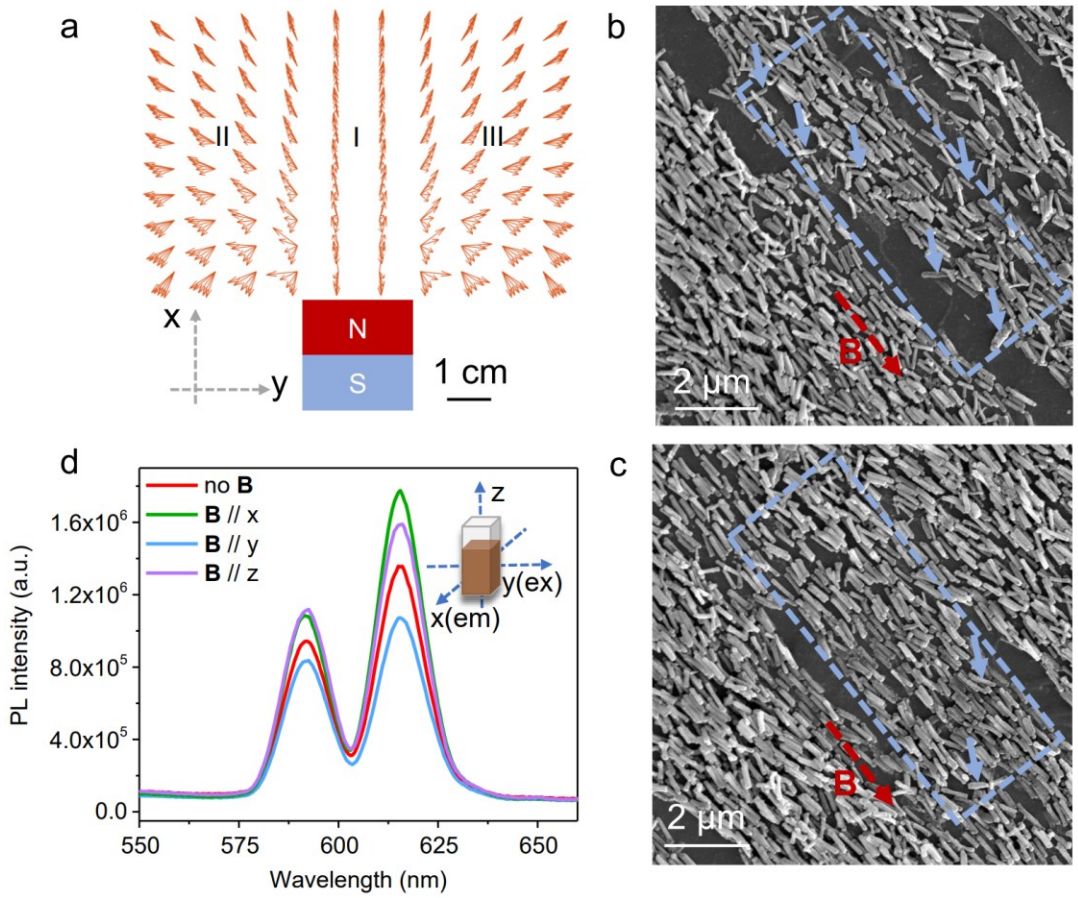

Figure 2. (a) Simulation of the chiral field distribution from a cubic permanent magnet; (b) The alignment of the composite nanorods under a chiral magnetic field; (c) The alignment of the composite nanorods under a uniform magnetic field; (d) PL spectra of composite nanorods (2 mg/mL in TEG) under magnetic fields of different directions or no magnetic field.

To investigate this angle-dependent emission behavior, the angle (θ) between the magnetic field direction and the y-axis was delicately changed in the x-y plane from 0° (along y) to 90° (along x). As shown in **Figure 3a** and **Figure 3b**, PL intensity increased gradually when the magnetic field direction changed from 0° to 90°. To explain the angle-dependent PL, absorption spectra were measured at corresponding magnetic field directions (**Figure 3c**). It could be seen that the absorbance of the Fe_3O_4-coated Eu-$NaYF_4$ nanorods increased gradually from 0° to 90°, in a way similar to the PL changes. This orientation-dependent absorption could only be attributed to the

anisotropic shape of Eu-$NaYF_4$ nanorods since the Fe_3O_4 NPs exhibit no angle-dependent absorption, as shown in **Figure S8**. When the composite nanorods were aligned along the x-axis (perpendicular to the propagation of excitation light), a larger absorption cross-section led to stronger absorption and photoluminescence.

It is worth noting that unlike those with large sizes (usually above 100 nm) and high local concentrations,[41] the Fe_3O_4 NPs in this study did not display observable angle-dependent absorption, likely due to their small sizes (below 10 nm on average) and low concentrations (which were estimated to be below 0.03 mg/mL via Beer's law by subtracting the absorbance of Eu-$NaYF_4$@PMAA from that of Eu-$NaYF_4$@PMAA@Fe_3O_4 (**Figure S4c**)).

When a chiral magnetic field was used, the self-assembly of Eu-$NaYF_4$@PMAA@Fe_3O_4 nanorods in TEG solution produced a strong circular dichroism (CD) signal due to the formation of chiral superstructures. Furthermore, the CD signal of the assembled superstructures also showed angular dependence in magnetic fields of different directions. The experimental setup of the CD measurement under different magnetic field directions was schemed in **Figure S9**. As shown in **Figure 3d**, the CD signal gradually increased when the magnetic field was rotated from 0° to 90°. According to Rosenfeld's theory, the CD chiroptical signal can be expressed by a single parameter R, which is equal to the dot product of electronic transition dipole moment $\boldsymbol{\mu}$ and magnetic transition dipole moment $\mathbf{m}$ ($R=\boldsymbol{\mu}\cdot\mathbf{m}=\mu m\cdot\cos\varphi$).[42-43] The rotation of the magnetic field could possibly result in the change of φ, which is the angle between $\boldsymbol{\mu}$ and $\mathbf{m}$ since the electron spin could produce an induced magnetic field.

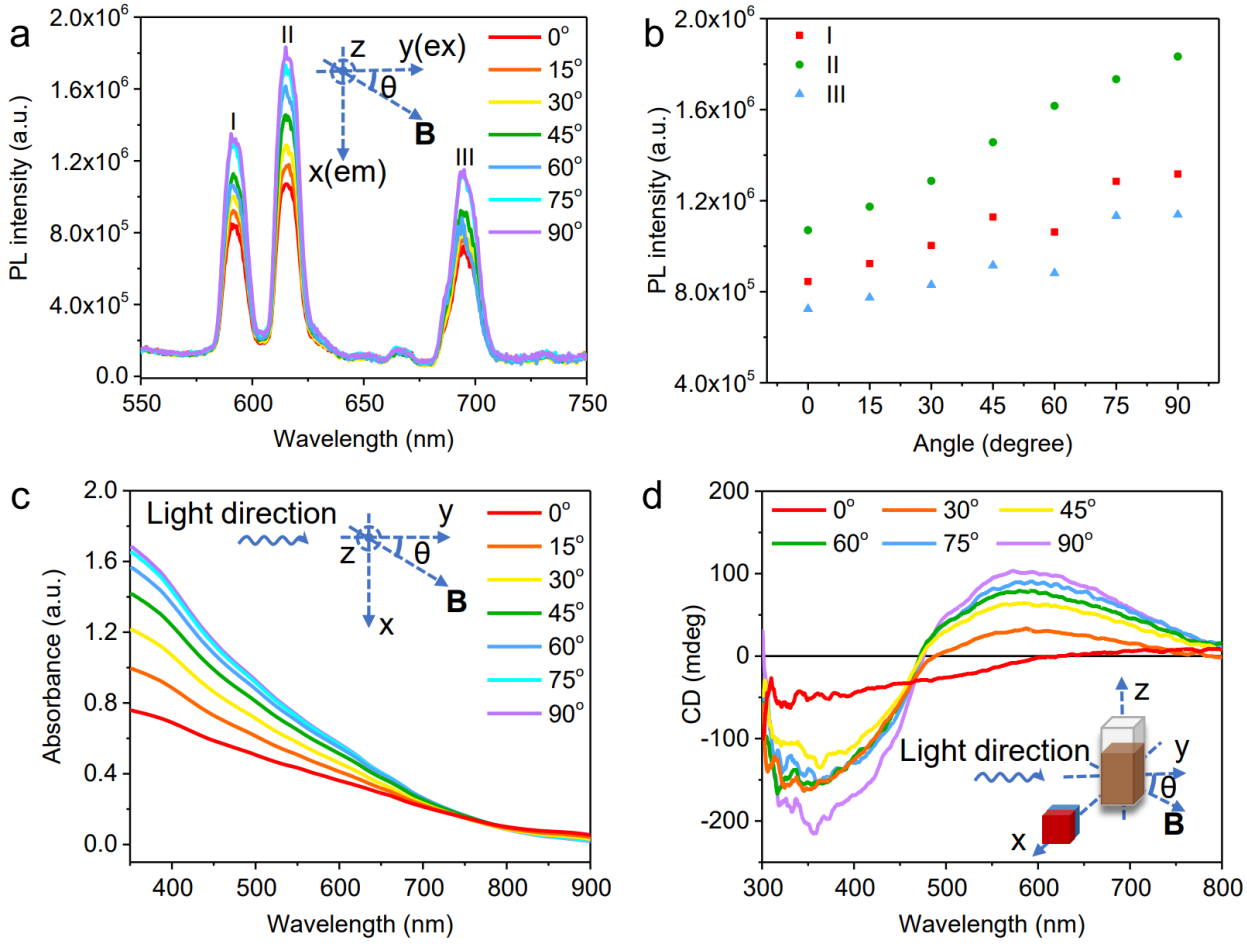

Figure 3. (a) PL spectra of composite nanorods (2 mg/mL in TEG) under magnetic fields of changing directions within the x-y plane; (b) Dependence of PL intensity of peak (I), (II) and (III) on field direction; (c) Absorption spectra of 1 mg/mL composite nanorods under magnetic fields of changing directions within the x-y plane; (d) CD spectra of the sample under magnetic fields of changing directions within the x-y plane.

To investigate their chiroptical properties further, we fixed the magnetically assembled chiral nanorod superstructures in a polyacrylamide (PAM) hydrogel through photopolymerization within a cuvette.[1] Consistent with the solution case, a strong CD signal was observed when the nanorods were parallel to the x-axis (perpendicular to light propagation) (**Figure 4a**). Notably, the peak at around 430 nm is caused by an artifact due to the detector saturation under this wavelength (**Figure**

S10). Interestingly, the CD signal of the hydrogel turned to an opposite sign but at the same magnitudes when the sample was flipped over by 180° (**Figure 4a**), indicating an opposite chirality. A similar chiral property was reported in an organic thin film.[44] According to a recent theoretical study,[45] such CD inversion phenomenon upon sample flipping could be explained by the linear dichroism (LD) and linear birefringence (LB) effect (LDLB effect, $CD_{obs} \approx CD + \frac{1}{2}$ (LD' • LB-LD • LB'), in which CD_{obs} represents the observed CD signal and prime sign means a 45° axis rotation. The sign of the second part in the formula will be reversed if the sample is flipped. When the LDLB effect is dominating in certain circumstances, such as samples with strong linear dichroism and linear birefringence, the sign of total CD signal could also be inverted by flipping over the samples. Additionally, the hydrogel displayed preferential absorption of either left-handed or right-handed circularly polarized light, contingent on its location within the left-handed or right-handed chiral magnetic field, yielding opposing CD spectra (**Figure S11a**).

As expected, this photoluminescent hydrogel with chirality exhibited obvious CPL and, more interestingly, inverted CPL when the sample was rotated by 180° (**Figure 4b**) regardless of whether the nanorods were along the x or y-axis. The CPL signals with inverted handedness indicate orientation-dependent circularly polarized emission, consistent with a chiral superstructure generated by the magnetic field. Corresponding to the opposite CD signal in **Figure S11a**, the chiral superstructure immobilized in the magnetic field with the opposite chirality also demonstrated inverted circularly polarized light emission (**Figure S11b**). It is worthwhile to note that when the nanorods were parallel to the x-axis, stronger CPL was observed with g_{lum} (defined as $2(I_L-I_R)/(I_L+I_R)$) up to 0.04 along the x-axis and 0.01 along the y-axis (**Figure S12**), consistent with the distinct chirality signals in different directions. Furthermore, from 587 to 597 nm, bisignate signals in the CPL spectra were observed, as labeled by the dash-squared region in

Figure 4b. Although a maximum of three transitions should be observed for the crystal field splitting of the $^5D_0 \rightarrow {}^7F_1$ transition,[46-47] only two transitions are resolved at 590 nm and 595 nm. The intensity of CD and CPL signals was proved to be contingent on the strength of the magnetic field. When a smaller magnet (4 mm) with a weaker intrinsic magnetic field strength (3 mT) was employed, the CD and CPL signals were considerably lower compared to the use of a 1-inch magnet (**Figure S13**).

Linear dichroism and linear birefringence are believed to play an important role in both the CD and CPL inversion upon sample overturn.[48] We measured the LD spectra of chiral superstructures assembled in PAM hydrogel in a cuvette (**Figure S14a**) and PAM hydrogel thin film (**Figure S14b**) based on LD= $A_{//}$-$A_{\perp}$, where $A_{//}$ and $A_{\perp}$ represent the absorbance when the polarizer is parallel and perpendicular to the orientation of nanorods, respectively.[49] The LD values of chiral superstructures are significant, albeit slightly smaller than those of linear superstructures.

The significant linear birefringence of nanorod assemblies was studied by aligning them under a chiral magnetic field, followed by fixation in a PAM hydrogel thin film (0.5 mm in thickness). The thin film fabrication process was explained in detail in the supporting information and schematically illustrated in **Figure S15a**. Similar nonreciprocal chirality was observed with the hydrogel thin film prepared under a chiral magnetic field. The handedness was found to be opposite when the film was measured from the front and back faces (**Figure S16**). The hydrogel thin film was observed under a polarized light microscope with two crossed polarizers and a rotating sample stage between them. It was found that the film brightness varied as the rotation angle changed. When the nanorods were 45° or 135° to the polarizer (P)/analyzer (A), the brightness was the highest, indicating the highest light transmission through the film (**Figure 4d**, **f**). When the nanorods were perpendicular or parallel to the polarizer/analyzer (0° or 90°), the brightness became

the lowest (**Figure 4c**, **e**). A lattice pattern of circles can be incorporated into the chiral hydrogel thin film using a lithography method (**Figure S15b**). The nanorods aligned inside and outside the circle areas are in 45° due to the 45-degree rotation of the magnetic field during UV-curing of these regions. Similarly, the circles became bright (nanorods inside the circles are 45° or 135° to the polarizer/analyzer) and dark (nanorods were perpendicular or parallel to the polarizer/analyzer) alternately under the polarized microscope when the film was rotated as shown in **Figure 4g**, **h**. These results are clear evidence of linear birefringence in the chiral hydrogel film,[15] which was sufficiently significant to allow the total CD and CPL inversion with sample reversal.

Since linear birefringence is the difference between its ordinary and extraordinary refractive indices (Δn),[50] we used the equation $I=I_0\sin^2(2\alpha)\sin^2(\pi\Delta nL/\lambda)$ to estimate the Δn of thin films observed under polarizing microscope, where I_0 is the intensity of light passing through the first polarizer; I is the intensity of light passing through the second polarizer; α is the angle between the transmission axes of the polarizer and the long axis of the thin film; L is the sample thickness; λ is the wavelength of incident light and Δn is the linear birefringence.[15] The linear birefringence of chiral and linear thin film was estimated to be 0.04 and 0.17, respectively.

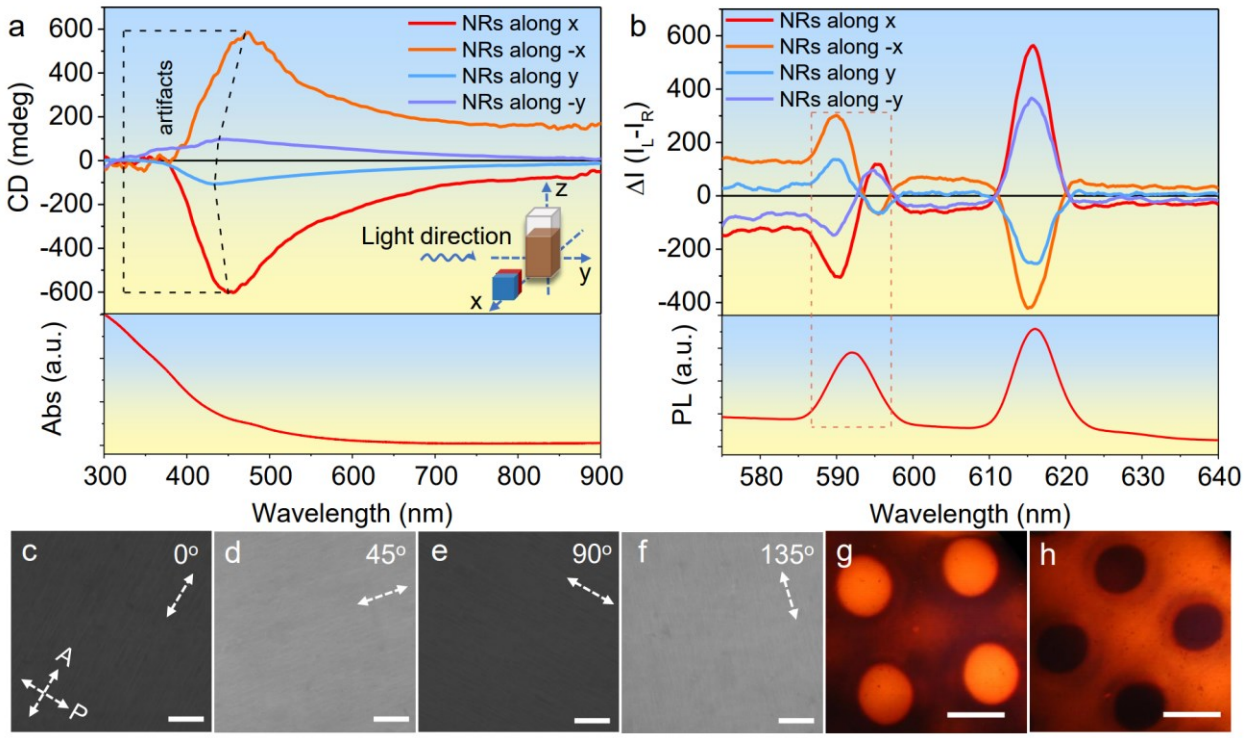

Figure 4. Chiroptical properties of Eu-$NaYF_4$@PMAA@Fe_3O_4 nanorods magnetically assembled in a hydrogel. The distance between the hydrogel and magnet is 1 cm, creating a magnetic field of 35 mT. (a, b) CD (a) and CPL (b) spectra of the hydrogel measured by flipping the sample; (c-f) Polarized light microscope images of a hydrogel thin film containing the magnetically assembled nanorods observed between a polarizer (P) and analyzer (A) in 90°. The relative orientations between the nanorods and polarizer/analyzer were labeled as dash lines; (g, h) Polarized light microscope images of a hydrogel thin film with a circle lattice pattern fabricated by the lithography method. The thin films were observed on a rotating sample stage sandwiched between the crossed polarizer and analyzer.

To gain a deeper insight into the disparity in chiroptical signals arising from the magnetic assembly in different orientations, we conducted theoretical simulations of the magnetic field distribution on a one-inch permanent cubic magnet, as illustrated in **Figure S17a**. Given that the incident light is directed along the y-axis, as shown in **Figure 4a** for the CD measurement, we compared the

magnetic field distribution in the x-z and y-z planes, as depicted in **Figures S17b** and **S17c**, respectively. Our analysis revealed a significant change in the field direction within the x-z plane, while only minimal changes in the field direction were observed in the y-z plane. Therefore, aligning the nanorods along the x-axis as opposed to the y-axis induced a greater rotation in response to the magnetic field, consequently resulting in a higher degree of chirality.[23]

The nanorods were aligned in a uniform magnetic field to obtain linear superstructures. **Figure 5a** shows that the linear superstructures aligned either along the x-axis or y-axis had no CD response due to the unidirectional alignment of the nanorods in the uniform field of opposing magnets (schemed in the insets of **Figure 5a**). Besides, no CPL signal was detected from the linear superstructure (**Figure S18**). The alignment of nanorods under chiral and uniform magnetic fields was compared through observations of hydrogel thin films using an optical microscope. We can observe twisting or crossing conformations within the chiral superstructure (**Figure S19a**), whereas the linear superstructure (**Figure S19b**) exhibits a more uniform alignment. To measure the LPL of the linear superstructure, we aligned the nanorods vertically by changing the magnetic field direction to z-direction while the polarization direction of the polarizer was also fixed vertically. By rotating the analyzer on the detection side, the angle between the nanorod c-axis and the electric field vector was changed, thereby allowing LPL measurement (see the setup scheme in **Figure S20**).[51] **Figures 5b** and **5c** show the PL intensity of the assemblies in TEG solution reached the maximum when the analyzer was parallel to the polarizer as well as the nanorods (0°, 180°, 360°, denoted as I_{VV}) and minimum at perpendicular positions (90°, 270°, denoted as I_{VH}). The solid fitting curves in **Figure 5c** indicate that the PL intensity changes with polarization angle, in good agreement with Malus law ($I(\theta)=(I_{VV}-I_{VH})\cos^2\theta+I_{VH}$).[52] The degree of polarization (DOP) calculated as $(I_{VV}-I_{VH})/(I_{VV}+I_{VH})$ was 0.50 for the peak at 591nm, 0.54 for the peak at 615 nm,

and 0.54 for the peak at 694 nm. A higher DOP up to 0.61 for the peak at 615 nm was obtained by fixing the nanorods in PAM hydrogel under a uniform magnetic field (**Figure S21** and **S22a**). The values of luminescence anisotropy (R) at different wavelengths calculated from (I_{VV}-I_{VH})/(I_{VV}+2I_{VH}) were listed in **Table S2**. Consistent with DOP, the highest R (0.51) was achieved at 615 nm for the assembly in PAM hydrogel. The polar plots of the magnetic self-assembly in TEG solution and PAM hydrogel are illustrated in **Figures 5d** and **S22b**, respectively, in which the solid curves represent the fitted PL intensities of the three PL peaks at different analyzer angles. Detailed information related to the LPL of self-assembly in TEG solution and PAM hydrogel is shown in **Table S3**. The DOP obtained in our magnetic assemblies was found to be higher than the $NaYF_4$ nanorods self-assembled using a shear-driven method.[11]

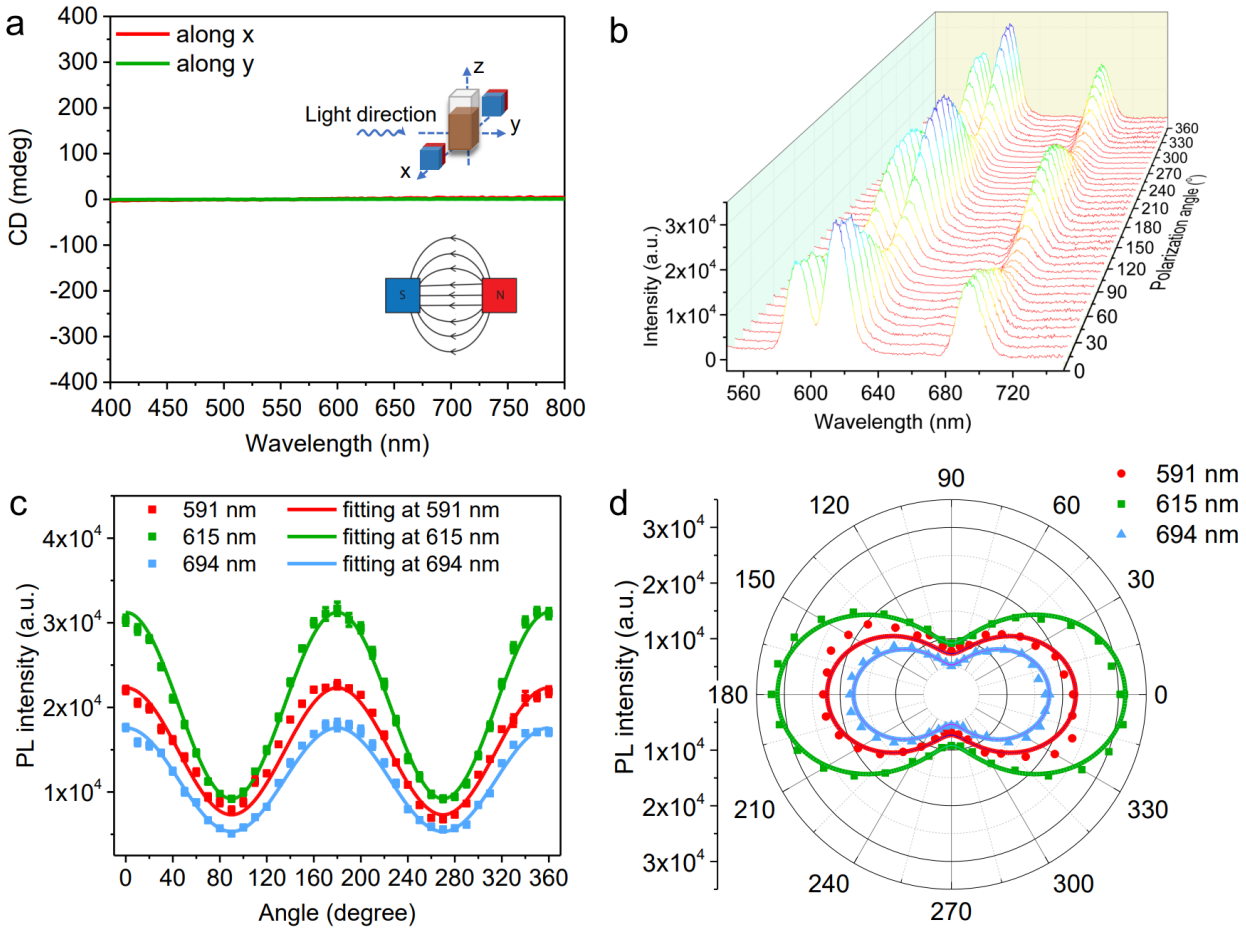

Figure 5. The LPL of Eu-$NaYF_4$@PMAA@Fe_3O_4 nanorods assembled in a linear magnetic field. (a) CD spectra of the superstructures assembled in TEG along the x-axis and y-axis in a uniform magnetic field; (b) PL spectra of the linear superstructures measured at different angles of the analyzer; (c) Change of peak intensity with polarization angle of the superstructures assembled in TEG in a uniform magnetic field; (d) Polar plot of the superstructures assembled in TEG in a uniform magnetic field.

CONCLUSION

In summary, we showcase the convenience and efficacy of the magnetic assembly approach in creating superstructures displaying CPL and LPL. By decorating the surface of fluorescent Eu-doped $NaYF_4$ nanorods with Fe_3O_4 nanoparticles, we demonstrate their successful assembly into linear and chiral superstructures in the corresponding fields of cubic permanent magnets. A uniform magnetic field created by two magnets with opposing polarities induces the unidirectional alignment of the nanorods, leading to LPL with DOP up to 0.61 and, more importantly, dynamically tunable emission intensity that can be controlled by the magnetic field direction. On the other hand, a quadrupolar chiral magnetic field of a cubic magnet assembles achiral nanorods into superstructures with high chirality, showing a distinct chirality signal depending on the relative spatial arrangement of the nanorods and the light propagation. The chiral superstructures exhibit left- or right-handed CPL with g_{lum} up to 0.04. Furthermore, a hydrogel film containing the as-assembled nanorods features the ability to inverse its chiroptical signals, including both CD and CPL, upon sample flipping, thanks to the significant linear birefringence of the nanorod assemblies. The magnetic assembly approach operates without the need for templates and exhibits versatile applicability across diverse luminescent materials. It enables instant and remote initiation,

positioning it as a promising avenue for developing optoelectronic devices that capitalize on the advantages of polarized emission.

METHODS

Eu-$NaYF_4$ nanorod (β phase) synthesis: The nanorods were prepared by following a hydrothermal process reported previously.[53] A typical synthesis started by mixing 700 mg NaOH with 8 mL oleic acid and then 12.7 mL ethanol. The mixture was stirred vigorously for 30 min to obtain a white viscous colloidal solution, followed by the dropwise addition of an aqueous NaF solution (12.45 mL, 0.58 M) to produce a clear solution. Then, a 1.5 mL aqueous solution containing 80 mol% $Y(NO_3)_3 \bullet 6H_2O$, 20 mol% $Eu(NO_3)_3 \bullet 6H_2O$ (1.2 mmol in total) was added to the system quickly. A white suspension was produced after stirring for 20 mins, which was transferred into a 50-mL Teflon-lined autoclave and heated at 230 ^oC for 12 hrs. The reaction led to the formation of nanorods, which were collected by centrifugation, cleaned with ethanol three times, and dried in a vacuum oven at 60 ^oC for 3 h. The as-prepared nanorods were sonicated in 10% TMAH solution for 30 min to remove the hydrophobic ligands of oleic acid. After that, the nanorods were collected by centrifugation and redispersed in water/ethanol (v:v=1:1), and the process was repeated another time. Finally, the nanorods were dried in a vacuum oven at 60 ^oC for 3 h.

Surface modification with γ-methacryloxypropyltrimethoxysilane (MPS): 250 mg ligand-free nanorods were dispersed in 20 mL ethanol in a round bottom flask, into which 5 mL deionized water, 300 μL ammonia solution (30 wt.%), and 200 mg MPS were added in sequence. The mixture was heated to 60 ^oC and kept for 6 h. After that, the nanorods were collected by centrifugation and washed with ethanol and water three times.

PMAA coating: The PMAA coating was achieved by a precipitation polymerization process.[34] The MPS-modified nanorods were dispersed into 20 mL acetonitrile in a single neck round bottom flask, followed by the addition of 25 mg N,N'-methylenebisacrylamide (MBA) as the cross-linking agent, 2.5 mg 2,2'-azobis(2-methylpropionitrile) (AIBN) as the initiator, and 100 μL MAA as the monomer. The mixture was heated at 90 ^{o}C in an oil bath for 1 h, evaporating 10 mL acetonitrile. The PMAA-coated nanorods were washed three times by centrifugation at 4000 rpm and ethanol redispersion to remove any free PMAA particles.

Fe_3O_4 decoration: Fe_3O_4 nanoparticles were coated by a simple co-precipitation method. The PMAA-coated $NaYF_4$ nanorods were dispersed in 20 mL of deionized water. Then 0.8 mmol anhydrous $FeCl_3$ and 0.4 mmol anhydrous $FeCl_2$ were added. The mixture was heated to 95 ^{o}C, followed by the quick injection of 5 mL 1 M NaOH aqueous solution. The reaction was kept at this temperature for 30 mins. The excess Fe_3O_4 nanoparticles were removed by repeated centrifugation at 3500 rpm for up to 5 times until the supernatant became clear and transparent. Then, the precipitate was redispersed in 10 mL water as a stock solution in a nominal concentration of 25 mg/mL for Eu-$NaYF_4$.

Preparation of poly(acrylamide) hydrogel: 250 mg acrylamide, 14 mg MBA, and 3 μL of the initiator 2-hydroxy-2-methylpropiophenone were added into 1 mL ethylene glycol. Then, the solution was cured under UV for 5 min to produce the PAM hydrogel. The Eu-$NaYF_4$@PMAA@Fe_3O_4 in different concentrations were added into the pre-gel solution to obtain composite hydrogels after UV curing. The thickness of the hydrogel films was determined by curing the pre-gel solution within a narrow space defined by two glass substrates and two PDMS spacers (0.5 mm in thickness). During UV curing, a permanent magnet was placed beside the hydrogel solution at varying distances of 1-3 cm to induce linear or chiral self-assembly. Patterns

were generated in the hydrogel thin film by covering the pre-gel solution film with a photomask. After curing for ~5 min, the photomask was removed. The magnetic field was rotated for 45°, followed by curing the film for another 5 min.

Optical characterizations: The UV-vis spectra were measured on a Cary-60 spectrometer or an Ocean Optics FLAME spectrometer with optic fibers. The PL spectra were measured on a Horiba QM-400 spectrometer. The CD spectra were measured on a Jasco J-815 spectrometer equipped with a built-in light source, photochromator, photo-elastic modulator, and detector, with a beam size of 1.5 mm and a wavelength range of 200-900 nm. The angle-dependent CD of the solution was measured by rotating the magnet within the CD spectrometer. CPL was measured on an Olis Solo UV-Vis spectrometer with a 380-nm LED light source, 0.25 nm step size, 1 s integration time, and 13 nm emission bandpass. A total of 100 scans were collected and averaged to produce the final data. Linear dichroism was obtained based on $LD=A_{//}-A_{\perp}$, where $A_{//}$ and $A_{\perp}$ represent the absorbance when the polarizer was parallel and perpendicular to the orientation of nanorods, respectively. The composite nanorods were aligned vertically under a chiral or uniform magnetic field, followed by the absorbance measurement with the polarizer parallel and perpendicular to the nanorods. The linear dichroism spectra were obtained by subtracting the spectrum with the perpendicular polarizer from the one with the parallel polarizer.

Microscopy characterization: Transmission electron microscopy was carried out on a Talos 120C system. Optical microscopy was performed on a Zeiss Axio microscope and a Keyence BZ-X710 microscope. The optical images with different magnetic field directions were taken by placing a magnet under the sample stage. Vertical and parallel magnetic fields could be created when the magnet was below and away from the sample. The polarized microscope images were taken by rotating the sample between the crossed polarizer and analyzer.

Magnetic field strength measurement: The magnetic field strength was measured by an HT20 Tesla meter.

ASSOCIATED CONTENT

Supporting Information

The Supporting Information is available free of charge.

Simulation methods of the magnetic field distribution; Excitation and emission of Eu-$NaYF_4$; TEM image, size distribution and absorption spectra of Fe_3O_4 NPs; TEM images of Eu-$NaYF_4$@PMAA at lower magnifications; absorption spectra of Eu-$NaYF_4$ throughout the surface treatment; TEM image and PL intensity with thick layer of Fe_3O_4 NPs; PL quenching due to magnetic separation; viscosity and magnetic separation time using different polyol solvents; optical images of magnetic responses of Eu-$NaYF_4$@PMAA@Fe_3O_4 nanorods; absorption spectra of Fe_3O_4 NPs under magnetic field with different directions; scheme of the experiment setup for CD measurements; high tension voltage of CD measurement; the CD and CPL spectra of the assembly in left-handed or right-handed magnetic field and using a smaller magnet; the g_{lum} of the PAM hydrogel; the scheme of hydrogel thin fil preparation; linear dichroism spectra of composite nanorods aligned in PAM hydrogels; fabrication of PAM hydrogel thin film and lithography processes; the CD signal of hydrogel thin film; the simulation results of magnetic field distribution; dark-field optical microscope images of Eu-$NaYF_4$@PMAA@Fe_3O_4 nanorod superstructure aligned in helical and uniform magnetic field; CPL spectra of linear superstructures; the experimental setup of LPL measurement; the LPL of Eu-$NaYF_4$@PMAA@Fe_3O_4 aligned in PAM hydrogel; the PL intensity and polar plot of the hydrogel containing the magnetic composite nanorods; the table showing the LPL information of solution and hydrogel.

AUTHOR INFORMATION

Author Contributions

The manuscript was written through contributions of all authors. All authors have given approval to the final version of the manuscript.

Funding Sources

This work was financially supported by the U.S. National Science Foundation (No. CHE-2203972).

Notes

The authors declare no competing financial interest.

ACKNOWLEDGMENT

The authors are grateful for the financial support from the U.S. National Science Foundation (No. CHE-2203972). Z.W. thanks Mr. Zuyang Ye for his help with hydrogel preparation, Dr. Ningning Song for her assistance with magnetic property measurement, and Dr. Adam Berges for his help with sample characterizations.

REFERENCES

1. Li, Z.; Jin, J.; Yang, F.; Song, N.; Yin, Y., Coupling Magnetic and Plasmonic Anisotropy in Hybrid Nanorods for Mechanochromic Responses. *Nat. Commun.* **2020,** *11*, 2883.

2. Gao, R.; Xu, L.; Hao, C.; Xu, C.; Kuang, H., Circular Polarized Light Activated Chiral Satellite Nanoprobes for the Imaging and Analysis of Multiple Metal Ions in Living Cells. *Angew. Chem. Int. Ed.* **2019,** *58*, 3913-3917.

3. Li, S.; Xu, L.; Ma, W.; Wu, X.; Sun, M.; Kuang, H.; Wang, L.; Kotov, N. A.; Xu, C., Dual-Mode Ultrasensitive Quantification of MicroRNA in Living Cells by Chiroplasmonic

Nanopyramids Self-Assembled from Gold and Upconversion Nanoparticles. *J. Am. Chem. Soc.* **2016,** *138*, 306-12.

4. Li, Z.; Ye, Z.; Han, L.; Fan, Q.; Wu, C.; Ding, D.; Xin, H. L.; Myung, N. V.; Yin, Y., Polarization-Modulated Multidirectional Photothermal Actuators. *Adv. Mater.* **2021,** *33*, e2006367.

5. Chen, Y.; Yang, X.; Gao, J., 3D Janus Plasmonic Helical Nanoapertures for Polarization-encrypted Data Storage. *Light Sci. Appl.* **2019,** *8*, 45.

6. Wang, X.; Wang, Y.; Gao, W.; Song, L.; Ran, C.; Chen, Y.; Huang, W., Polarization-Sensitive Halide Perovskites for Polarized Luminescence and Detection: Recent Advances and Perspectives. *Adv. Mater.* **2021,** *33*, e2003615.

7. Jiang, S.; Kotov, N. A., Circular Polarized Light Emission in Chiral Inorganic Nanomaterials. *Adv. Mater.* **2023,** *35*, 2108431.

8. Sang, Y.; Han, J.; Zhao, T.; Duan, P.; Liu, M., Circularly Polarized Luminescence in Nanoassemblies: Generation, Amplification, and Application. *Adv. Mater.* **2020,** *32*, e1900110.

9. Han, D.; Li, C.; Jiang, C.; Jin, X.; Wang, X.; Chen, R.; Cheng, J.; Duan, P., Endowing Inorganic Nanomaterials with Circularly Polarized Luminescence. *Aggregate* **2021,** *3*, e148.

10. Rong, S.; Shi, W.; Zhang, S.; Wang, X., Circularly and Linearly Polarized Luminescence from AIE Luminogens Induced by Super-aligned Assemblies of Sub-1 nm Nanowires. *Angew. Chem. Int. Ed.* **2022,** *61*, e202208349.

11. He, H.; Liu, J.; Li, K.; Yin, Z.; Wang, J.; Luo, D.; Liu, Y. J., Linearly Polarized Emission from Shear-Induced Nematic Phase Upconversion Nanorods. *Nano Lett.* **2020,** *20*, 4204-4210.

12. Shi, Y.; Duan, P.; Huo, S.; Li, Y.; Liu, M., Endowing Perovskite Nanocrystals with Circularly Polarized Luminescence. *Adv. Mater.* **2018,** *30*, e1705011.

13. Jin, X.; Sang, Y.; Shi, Y.; Li, Y.; Zhu, X.; Duan, P.; Liu, M., Optically Active Upconverting Nanoparticles with Induced Circularly Polarized Luminescence and Enantioselectively Triggered Photopolymerization. *ACS Nano* **2019,** *13*, 2804-2811.

14. Wang, M.; Yin, Y., Magnetically Responsive Nanostructures with Tunable Optical Properties. *J. Am. Chem. Soc.* **2016,** *138*, 6315-23.

15. Wang, M.; He, L.; Zorba, S.; Yin, Y., Magnetically Actuated Liquid Crystals. *Nano Lett.* **2014,** *14*, 3966-3971.

16. Li, Z.; Qian, C.; Xu, W.; Zhu, C.; Yin, Y., Coupling Morphological and Magnetic Anisotropy for Assembling Tetragonal Colloidal Crystals. *Sci. Adv.* **2021,** *7*, eabh1289.

17. Wang, M.; He, L.; Yin, Y., Magnetic Field Guided Colloidal Assembly. *Mater. Today* **2013,** *16*, 110-116.

18. He, L.; Wang, M.; Ge, J.; Yin, Y., Magnetic Assembly Route to Colloidal Responsive Photonic Nanostructures. *Acc. Chem. Res.* **2012,** *45*, 1431–1440.

19. Li, Z.; Yang, F.; Yin, Y., Smart Materials by Nanoscale Magnetic Assembly. *Adv. Funct. Mater.* **2019,** *30*, 1903467.

20. Fan, Q.; Li, Z.; Wu, C.; Yin, Y., Magnetically Induced Anisotropic Interaction in Colloidal Assembly. *Precis. Chem.* **2023,** *1*, 272-298.

21. Singh, G.; Chan, H.; Baskin, A.; Gelman, E.; Repnin, N.; Král, P.; Klajn, R., Self-assembly of Magnetite Nanocubes into Helical Superstructures. *Science* **2014,** *345*, 1149-1153.

22. Jeong, K. J.; Lee, D. K.; Tran, V. T.; Wang, C.; Lv, J.; Park, J.; Tang, Z.; Lee, J., Helical Magnetic Field-Induced Real-Time Plasmonic Chirality Modulation. *ACS Nano* **2020,** *14*, 7152-7160.

23. Li, Z.; Fan, Q.; Ye, Z.; Wu, C.; Wang, Z.; Yin, Y., A Magnetic Assembly Approach to Chiral Superstructures. *Science* **2023,** *380*, 1384-1390.

24. Liu, Y.; Tu, D.; Zhu, H.; Chen, X., Lanthanide-doped Luminescent Nanoprobes: Controlled Synthesis, Optical Spectroscopy, and Bioapplications. *Chem. Soc. Rev.* **2013,** *42*, 6924-6958.

25. Liu, Y.; Tang, A.; Zhang, Q.; Yin, Y., Seed-Mediated Growth of Anatase TiO_2 Nanocrystals with Core-Antenna Structures for Enhanced Photocatalytic Activity. *J. Am. Chem. Soc.* **2015,** *137*, 11327-39.

26. Zeng, J.; Gong, M.; Wang, D.; Li, M.; Xu, W.; Li, Z.; Li, S.; Zhang, D.; Yan, Z.; Yin, Y., Direct Synthesis of Water-Dispersible Magnetic/Plasmonic Heteronanostructures for Multimodality Biomedical Imaging. *Nano Lett.* **2019,** *19*, 3011-3018.

27. Chen, X.; Ye, Z.; Yang, F.; Feng, J.; Li, Z.; Huang, C.; Ke, Q.; Yin, Y., Magnetic Cellulose Microcrystals with Tunable Magneto-optical Responses. *Appl. Mater. Today* **2020,** *20*, 100749.

28. Wang, C.; Chen, J.; Talavage, T.; Irudayaraj, J., Gold Nanorod/Fe_3O_4 Nanoparticle "Nano-pearl-necklaces" for Simultaneous Targeting, Dual-mode Imaging, and Photothermal Ablation of Cancer Cells. *Angew. Chem. Int. Ed.* **2009,** *48*, 2759-63.

29. Duan, S.; Li, J.; Zhao, N.; Xu, F. J., Multifunctional Hybrids with Versatile Types of Nanoparticles via Self-assembly for Complementary Tumor Therapy. *Nanoscale* **2018,** *10*, 7649-7657.

30. Ahn, M. S.; Ahmad, R.; Bhat, K. S.; Yoo, J. Y.; Mahmoudi, T.; Hahn, Y. B., Fabrication of a Solution-gated Transistor Based on Valinomycin Modified Iron Oxide Nanoparticles Decorated Zinc Oxide Nanorods for Potassium Detection. *J. Colloid. Interf. Sci.* **2018,** *518*, 277-283.

31. Liu, K.; Han, L.; Tang, P.; Yang, K.; Gan, D.; Wang, X.; Wang, K.; Ren, F.; Fang, L.; Xu, Y.; Lu, Z.; Lu, X., An Anisotropic Hydrogel Based on Mussel-Inspired Conductive Ferrofluid Composed of Electromagnetic Nanohybrids. *Nano Lett.* **2019,** *19*, 8343-8356.

32. Yuan, J.; Gao, H.; Schacher, F.; Xu, Y.; Richter, R.; Tremel, W.; Müller, A. H. E., Alignment of Tellurium Nanorods via a Magnetization−Alignment− Demagnetization ("MAD") Process Assisted by an External Magnetic Field. *ACS Nano* **2009,** *3*, 1441-1450.

33. Rizvi, M. H.; Wang, R.; Schubert, J.; Crumpler, W. D.; Rossner, C.; Oldenburg, A. L.; Fery, A.; Tracy, J. B., Magnetic Alignment for Plasmonic Control of Gold Nanorods Coated with Iron Oxide Nanoparticles. *Adv. Mater.* **2022,** *34*, e2203366.

34. Ma, W.; Xu, S.; Li, J.; Guo, J.; Lin, Y.; Wang, C., Hydrophilic Dual-responsive Magnetite/PMAA Core/shell Microspheres with High Magnetic Susceptibility and pH Sensitivity via Distillation-precipitation Polymerization. *J. Polym. Sci., Part A: Polym. Chem.* **2011,** *49*, 2725-2733.

35. Wang, L.; Li, Y., Controlled Synthesis and Luminescence of Lanthanide Doped $NaYF_4$ Nanocrystals. *Chem. Mater.* **2007,** *19*, 727-734.

36. Wang, Z.; Tai, Y.; Nam, J.; Yin, Y., Calcination-Induced Transformation of $ZnS:Mn^{2+}$ Nanorods to Microparticles for Enhanced Mechanoluminescence. *Chem. Mater.* **2023,** *35*, 6845-6852.

37. Li, R.; Fang, X.; Ren, J.; Chen, B.; Yuan, X.; Pan, X.; Zhang, P.; Zhang, L.; Tu, D.; Fang, Z.; Chen, X.; Ju, Q., The Effect of Surface-capping Oleic Acid on the Optical Properties of Lanthanide-doped Nanocrystals. *Nanoscale* **2021,** *13*, 12494-12504.

38. Hassinen, A.; Moreels, I.; De Nolf, K.; Smet, P. F.; Martins, J. C.; Hens, Z., Short-chain Alcohols Strip X-type Ligands and Quench the Luminescence of PbSe and CdSe Quantum Dots, Acetonitrile Does Not. *J. Am. Chem. Soc.* **2012,** *134*, 20705-12.

39. Wang, Z.; Long, P.; Feng, Y.; Qin, C.; Feng, W., Surface Passivation of Carbon Dots with Ethylene Glycol and Their High-sensitivity to Fe^{3+}. *RSC Adv.* **2017,** *7*, 2810-2816.

40. Ye, Z.; Li, Z.; Feng, J.; Wu, C.; Fan, Q.; Chen, C.; Chen, J.; Yin, Y., Dual-Responsive Fe(3)O(4)@Polyaniline Chiral Superstructures for Information Encryption. *ACS Nano* **2023,** *17*, 18517-18524.

41. Zhang, X.; Li, Z.; Feng, J.; Yang, F.; Wu, C.; Fan, Q.; Zhou, S.; Yin, Y., Dynamic Tuning of Optical Transmittance of 1D Colloidal Assemblies of Magnetic Nanostructures. *Adv. Intell. Syst.* **2019,** *1*, 1900099.

42. Zinna, F.; Di Bari, L., Lanthanide Circularly Polarized Luminescence: Bases and Applications. *Chirality* **2015,** *27*, 1-13.

43. Tanaka, H.; Inoue, Y.; Mori, T., Circularly Polarized Luminescence and Circular Dichroisms in Small Organic Molecules: Correlation between Excitation and Emission Dissymmetry Factors. *ChemPhotoChem* **2018,** *2*, 386-402.

44. Albano, G.; Lissia, M.; Pescitelli, G.; Aronica, L. A.; Di Bari, L., Chiroptical Response Inversion upon Sample Flipping in Thin Films of a Chiral Benzo[1,2-b:4,5-b]dithiophene-based Oligothiophene. *Mater. Chem. Front.* **2017,** *1*, 2047-2056.

45. Salij, A.; Goldsmith, R. H.; Tempelaar, R., Theory of Apparent Circular Dichroism Reveals the Origin of Inverted and Noninverted Chiroptical Response under Sample Flipping. *J. Am. Chem. Soc.* **2021,** *143*, 21519-21531.

46. Mukthar, N. F. M.; Schley, N. D.; Ung, G., Strong Circularly Polarized Luminescence at 1550 nm from Enantiopure Molecular Erbium Complexes. *J. Am. Chem. Soc.* **2022,** *144*, 6148-6153.

47. Wu, T.; Kessler, J.; Bour, P., Chiral Sensing of Amino Acids and Proteins Chelating with Eu(III) Complexes by Raman Optical Activity Spectroscopy. *Phys. Chem. Chem. Phys.* **2016,** *18*, 23803-11.

48. Zinna, F.; Albano, G.; Taddeucci, A.; Colli, T.; Aronica, L. A.; Pescitelli, G.; Di Bari, L., Emergent Nonreciprocal Circularly Polarized Emission from an Organic Thin Film. *Adv. Mater.* **2020,** *32*, e2002575.

49. Bulheller, B. M.; Rodger, A.; Hirst, J. D., Circular and Linear Dichroism of Proteins. *Phys. Chem. Chem. Phys.* **2007,** *9*, 2020-35.

50. Dorohoi, D. O.; Postolache, M.; Nechifor, C. D.; Dimitriu, D. G.; Albu, R. M.; Stoica, I.; Barzic, A. I., Review on Optical Methods Used to Characterize the Linear Birefringence of Polymer Materials for Various Applications. *Molecules* 2023, 28, 2955.

51. Chen, P.; Song, M.; Wu, E.; Wu, B.; Zhou, J.; Zeng, H.; Liu, X.; Qiu, J., Polarization Modulated Upconversion Luminescence: Single Particle vs. Few-particle Aggregates. *Nanoscale* **2015,** *7*, 6462-6466.

52. Zhang, J.; Meng, C.; Huang, J.; Jiang, L.; Zhou, D.; Chen, R.; Yeung, F.; Kwok, H. S.; Xu, P.; Li, G., Strong Linearly Polarized Photoluminescence and Electroluminescence from Halide Perovskite/Azobenzene Dye Composite Film for Display Applications. *Adv. Opt. Mater.* **2020,** *8*, 1901824.

53. Zhou, J.; Chen, G.; Wu, E.; Bi, G.; Wu, B.; Teng, Y.; Zhou, S.; Qiu, J., Ultrasensitive Polarized Up-conversion of Tm(3+)-Yb3+ Doped Beta-$NaYF_4$ Single Nanorod. *Nano Lett.* **2013,** *13*, 2241-2246.

TOC Graphic:

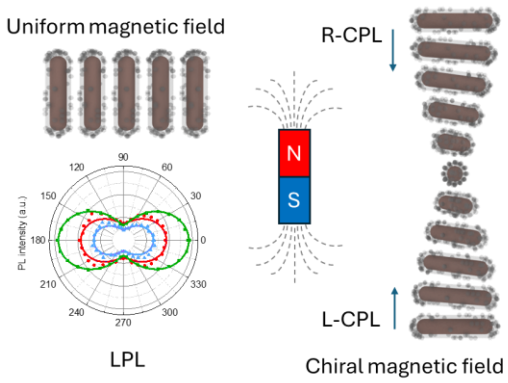
Uniform magnetic field
90
120
60
150
30
180
0
210
330
240
300
270
PL intensity (a.u.)
LPL
N
S
R-CPL
L-CPL
Chiral magnetic field